

Electronic Supplementary Information

Titanate Nanotube-Promoted Chemical Fixation of Carbon Dioxide to Cyclic Carbonate: A Combined Experimental and Computational Study

Aibing Chen,^a Tiancong Zhao,^{a,b} Hui Gao,^b Limin Chen,^c Jinzhu Chen,^{*b} and
Yifeng Yu^a

^a College of Chemical and Pharmaceutical Engineering, Hebei University of Science and Technology, Shijiazhuang 050018 (PR China)

^b CAS Key Laboratory of Renewable Energy, Guangzhou Institute of Energy Conversion, Chinese Academy of Sciences, Guangzhou 510640 (PR China)

^c School of Environment and Energy, South China University of Technology, Guangzhou Higher Education Mega Centre, Guangzhou 510006 (PR China)

* Corresponding author. Tel./Fax: (+86)-20-3722-3380. E-mail address: chenjz@ms.giec.ac.cn (J. Chen)

1. Experimental

1.1. Chemicals

Unless otherwise stated, all chemicals in this work were commercial available and used without further purification. HCl (36~38 wt.% aqueous solution), CaCl₂ and methylbenzene were purchased from Sinopharm Chemical Reagent Co. Ltd. (Shanghai, P. R. China). 1,2-Epoxypropane and dichloromethane (CH₂Cl₂) were purchased from Shanghai Lingfeng Chemical Reagent Co. Ltd. (Shanghai, P. R. China). Ethanol and cupric chloride (CuCl₂) were purchased from Guangdong Guanghua Sci-Tech Co. Ltd. (Guangzhou, P. R. China). Oleic acid and cobalt chloride (CoCl₂) were purchased from Tianjin Kemiou Chemical Reagent Co. Ltd. (Tianjin, P. R. China). Tetrabutyl ammonium bromide (TBAB) and tetraphenylphosphonium bromide (TPPB) were purchased from Aladdin Industrial Inc. (Shanghai, P. R. China). P25 was purchased from Guangzhou Hualisen Trading Co. Ltd. (Guangzhou, P. R. China). KI was purchased from Shanghai Yindian Chemical Co. Ltd. (Shanghai, P. R. China). NaOH was purchased from Nanjing Chemical Reagent Co. Ltd. (Nanjing, P. R. China). ZnCl₂ was purchased from Shanghai Qiangshun Chemical Reagent Co. Ltd. (Shanghai, P. R. China). Mg(NO₃)₂ was purchased from Guangzhou Chemical Reagent Factory (Guangzhou, P. R. China). Deionized pure water was made from Millipore-Milli Q Plus System.

1.2. Synthesis of TNT

In this study, we synthesized titanate nanotubes (TNT) through hydrothermal method which had been reported.^[1] As-received P25 (500 mg) and concentrated NaOH solution (10 M, 50 mL) were placed into a Teflon container which was under mild stirring before the mixture was blend well and then it was heated at 140 °C for 24 h; the resultant white precipitate was then separated from the mixture by centrifugation and washed with deionized pure water, HCl solution (0.1 M) and ethanol several times until the pH of the solution was almost 7. Finally, the powder was dried at 30 °C under vacuum for 8 h.

1.3. Synthesis of metal-doped TNT (M-TNT)

The deposition-precipitation method The way to prepare M-TNT catalysts was used.^[1b,2] The TNT (200 mg) was dissolved in CoCl₂, ZnCl₂, CuCl₂, MgNO₃, CaCl₂, (0.05 mol L⁻¹ 200 mL) aqueous solution. Then the solution's pH value was set to 7. After that, the mixture was stirred for 24 h at 25 °C. The products (Zn-TNT, Cu-TNT, Mg-TNT, Ca-TNT) were then centrifuged, filtered and washed with distilled water, alcohol until no chlorides. The final products was dried at 80 °C for 6 h.

1.4. Recycling experiments

The reusability of TNT was tested for synthesis of popylene carbonate under the same reaction conditions as described in the experiment of general procedure for cycloaddition reaction of CO₂ to propylene oxide. Each time the TNT was washed with ethanol, dionized pure water several times until all impurities was removed. And then dry the powder at 80 °C under vacuum 8 h. It is important to highlight that nearly identical results were achieved after four recycles.

2. Characterization

BET surface area measurements were performed with N₂ adsorption/desorption isotherms at 77 K (SI-MP-10/PoreMaster 33, Quantachrome). Before the analysis, samples were outgassed at 150 °C for 20 h. Surface area, micropore volume and pore diameters were obtained by Brunauer-Emmet-Teller (BET), Barrett-Joyner-Halenda (BJH) desorption pore volume and BJH desorption pore size methods, respectively.

Fourier transform infrared (FT-IR) spectra of KBr wafers were recorded at room temperature in

the 500-2200 cm^{-1} region with a Bruker Tensor 27 spectrometer, equipped with a Data Station, at a spectral resolution of 1 cm^{-1} and accumulations of 128 scans.

IR spectra of pyridine adsorbed (Py-IR) were carried out using a Bruker Tensor 27 spectrometer, equipped with a Data Station and a BX-5 in situ transmit infrared quartz stainless steel clad reactor. The text method was as followed, weighed samples of about 20 mg, tablet a ϕ 13 mm sheet, and placed in a quartz sample cuvette in the sample compartment, under a vacuum of 1.0×10^{-3} Pa state after 200 $^{\circ}\text{C}$ activation 2 h later reduced to 40 $^{\circ}\text{C}$, single-channel collection background spectra. Then pyridine adsorption 20 min, 30 min after desorption equilibrium vacuum pump and IR scan to 10 $^{\circ}\text{C min}^{-1}$ to rise 150 $^{\circ}\text{C}$ balanced 30 min, collect the sample spectrum; to 10 $^{\circ}\text{C min}^{-1}$ to rise to 400 $^{\circ}\text{C}$ balanced 30 min, collected sample spectrum.

The morphological analysis and nanoparticle size and distribution were carried out using transmission electron microscopy (TEM, JEM-2100HR). Samples for TEM and HRTEM studies were prepared by placing a drop of the suspension of TNTs sample in ethanol onto a carbon-coated copper grid, followed by evaporating the solvent. To obtain the particle size distribution diagram and an accurate estimation of the average particle size, more than 250 particles for each catalyst were manually counted.

Powder X-ray diffraction (XRD) patterns of TNTs were obtained with a PANalytical X'pert Pro MPD diffractometer operated at 40 KV and 40 mA, using Ni-filtered $\text{Cu-K}\alpha$ radiation.

X-ray photoelectron spectroscopy (XPS) spectra was performed with a Kratos Axis Ultra (DLD) photoelectron spectrometer operated at 15 kV and 10 mA at a pressure of about 5×10^{-9} torr using $\text{AlK}\alpha$ as the exciting source ($h\nu = 1486.6\text{eV}$). C 1s photoelectron peak ($\text{BE} = 284.2\text{ eV}$) was used for the binding energy calibration.

Thermogravimetric analysis (TGA) was carried out on a Shimadzu TGA-50 instrument. The samples were heated from room temperature to 800 $^{\circ}\text{C}$ under a nitrogen flow of 20 mL min^{-1} at a heating rate of 10 $^{\circ}\text{C min}^{-1}$.

3. Computational Details

The theoretical calculations were performed in Gaussian 09 program³ using B3LYP functional⁴. The basis set 6-311++G(d,p) for I atoms and SDD⁵ for other atoms were used. Frequency analyses were done in order to ensure that the optimized structures were at either a minimum or transition state. The thermodynamic functions, including the enthalpies and free energies, were calculated at 298.15 K and 1 atm. The intrinsic reaction coordinate (IRC) method⁶ was performed to confirm the transition states found connected relevant reactants and products. All the reported structures were fully optimized using the polarizable continuum model (PCM) method⁷ with SMD⁸ atomic radii for experimental solvent (CH_2Cl_2).

The uncatalyzed cycloaddition reaction: In the absence of catalyst, the cycloaddition of CO_2 to PO to form PC via a one-step transition-state (TS_{uncat}), which corresponds to the simultaneous breaking of the C–O bond of the PO and the simultaneous formation of two new C–O bonds that originate from the insertion of CO_2 (Fig. 1). The free energy barrier is about 48.3 $\text{kcal}\cdot\text{mol}^{-1}$ (similar to the previous reports⁹⁻¹⁰), suggesting that the reaction is very difficult to process without extra catalysts, which is also reflected by our experimental observation that the PC yield is 0% in the absence of catalysts.

The only KI catalyzed cycloaddition reaction: In the presence of KI, the catalytic mechanism proceeds two steps: one is breaking of the C–O bond of the PO and the other is ring

closing of PC (Fig. 2). The K^+ cation interacts with the oxygen atom of PO and one of oxygen atom in CO_2 to form initial structure (**RC_{KI}**). Firstly, with the attack of carbon atom in CO_2 to the O atom of PO, the C–O bond of the PO is breaking in TS1. The free energy barrier for this step is $40.7 \text{ kcal mol}^{-1}$ (similar to the previous reports⁹⁻¹⁰). Through the **TS1_{KI}**, an intermediate **IM_{KI}** with the free energy of $16.0 \text{ kcal mol}^{-1}$ is formed. In **IM_{KI}**, the new C–O bond and C–I bond formed. Then, with the attack of the other oxygen atoms of CO_2 to the side of the C–I bond, the intramolecular cyclic step is occurred via **TS2_{KI}** with the free energy of $35.2 \text{ kcal mol}^{-1}$. The calculation shows that the simultaneous epoxy ring opening and the electrophilic attack of CO_2 is the rate-determining step, in which the barrier is $7.6 \text{ kcal mol}^{-1}$ lowered than that of the uncatalyzed reaction, suggesting that the KI can promoted the reaction. However, the free energy barrier of $40.7 \text{ kcal mol}^{-1}$ is still too high to overcome, which indicate that the reaction is very difficult to process even if in the presence of KI. The calculations are also well reflected by our experimental observation that the PC yield is only 1.0% in the presence of only KI.

The only $H_2Ti_2O_5$ catalyzed cycloaddition reaction: In the presence of $H_2Ti_2O_5$, the cycloaddition reaction pathway of CO_2 to PO is depicted in Fig. 3, in which the sum of free energies of the isolated reactants (PO+ CO_2) and $H_2Ti_2O_5$ were set to zero. The initial step is the coordination of the epoxide to the $H_2Ti_2O_5$, which forms an initial structure (**RC_{Ti}**), followed by a concerted ring-opening. The transition state **TS1_{Ti}** relates to the simultaneous stretching/breaking of the C–O bond of the epoxide. Through the **TS1_{Ti}**, an intermediate **IM_{Ti}** with the free energy of $11.5 \text{ kcal mol}^{-1}$ is formed. Subsequently, the bending of the CO_2 molecule leads to the formation of two new C–O bonds via a transition state **TS2_{Ti}** with the free energy of $29.2 \text{ kcal mol}^{-1}$. The relative potential energy barrier for the $H_2Ti_2O_5$ -catalyzed cycloaddition is reduced by $19.1 \text{ kcal mol}^{-1}$ compared with the uncatalyzed reaction, which is likely as a result of the formation of a $H_2Ti_2O_5$ /epoxide polarizing the C–O bond of the substrate and thus playing an important role in its activation. The calculations suggest that the $H_2Ti_2O_5$ can promote the reaction, which are also well reflected by our experimental observation that only 8.0% PC yield in the presence of only $H_2Ti_2O_5$.

1. T. Kasuga, M. Hiramatsu, A. Hoson, T. Sekino, and K. Niihara, *Adv. Mater.* 1999, **11**, 1307; (b) X. M. Sun and Y. D. Li, *Chem. Eur. J.*, 2003, **9**, 2229; (c) J. G. Yu, H. G. Yu, B. Cheng and C. Trapalis, *J. Mol. Catal. A: Chem.*, 2006, **249**, 135.
2. A. Primo, P. Concepcion and A. Corma, *Chem. Commun.*, 2011, **47**, 3613.
3. M. J. Frisch, et al., Revision C.01, Gaussian, Inc., Wallingford CT, 2010.
4. (a) A. D. J. Becke, *Chem. Phys.* 1993, **98**, 5648; (b) C. Lee, W. Yang and R. G. Parr, *Phys. Rev. B* 1988, **37**, 785.
5. (a) Roy, L. E.; Hay, P. J.; Martin, R. L. *J. Chem. Theory Comput.* 2008, **4**, 1029. (b) Andrae, D.; Haussermann, U.; Dolg, M.; Stoll, H.; Preuss, H. *Theor. Chem. Acc.* 1990, **77**, 123.
6. (a) C. Gonzalez and H. B. Schlegel, *J. Phys. Chem.*, 1990, **94**, 5523; (b) C. Gonzalez and H. B. Schlegel, *J. Chem. Phys.*, 1989, **90**, 2154.
7. A. V. Marenich, C. J. Cramer and D. G. Truhlar, *J. Phys. Chem. B*, 2009, **113**, 6378.
8. J. Tomasi, B. Mennucci and R. Cammi, *Chem. Rev.*, 2005, **105**, 2999.
9. F. Castro-Gómez, G. Salassa, A. W. Kleij and C. Bo, *Chem. Eur. J.* 2013, **19**, 6289.
10. J. Ma, J. Liu, Z. Zhang and B. Han, *Green Chem.* 2012, **14**, 2410.

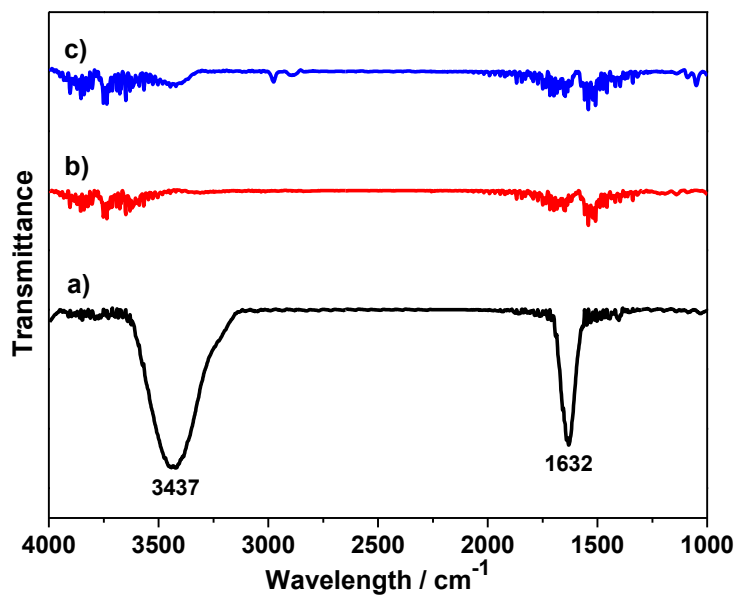


Figure S3. FT-IR spectra of (a) TNT, (b) P25, and (c) TiO₂

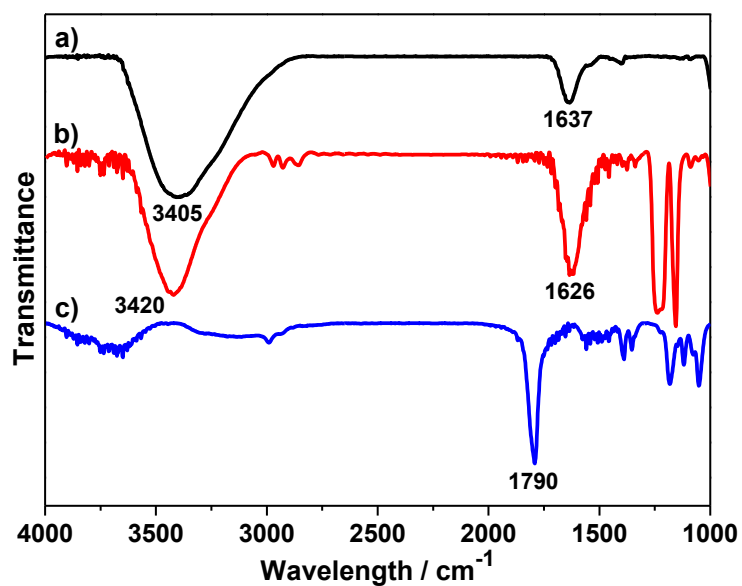


Figure S4. FT-IR spectra of (a) TNT300, (b) recovered TNT300 with the reaction conditions described in Figure 12, and (c) PC.

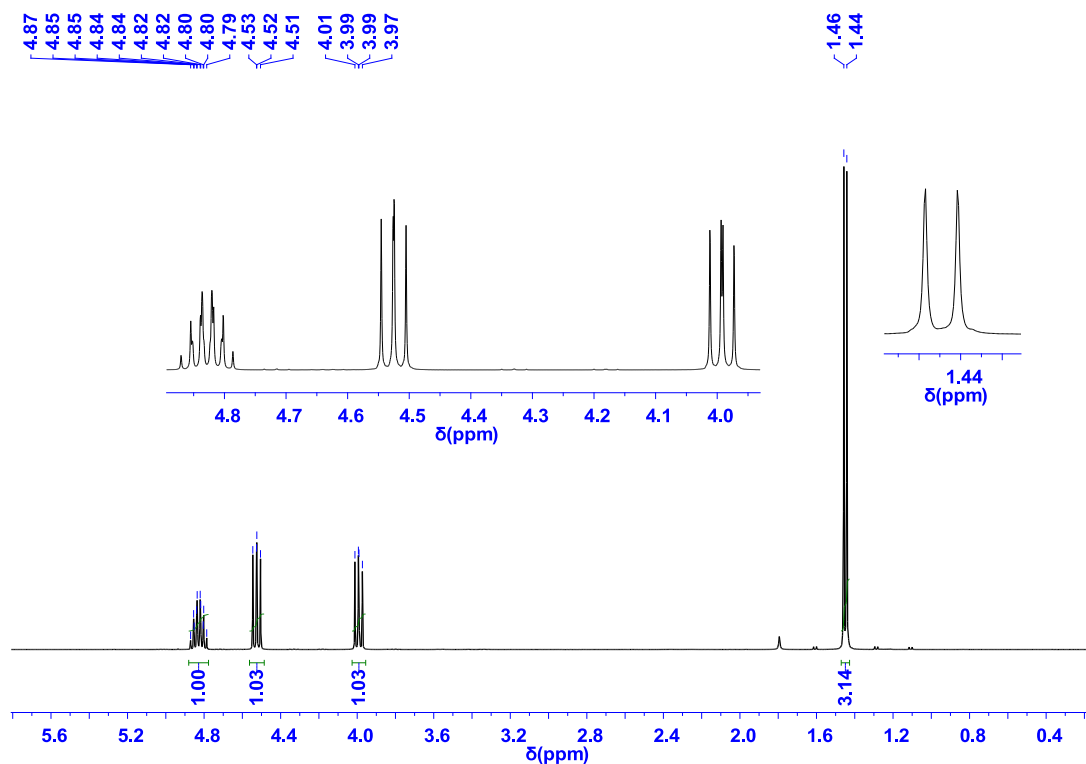


Figure S5. ^1H NMR of propylene carbonate in CDCl_3 .

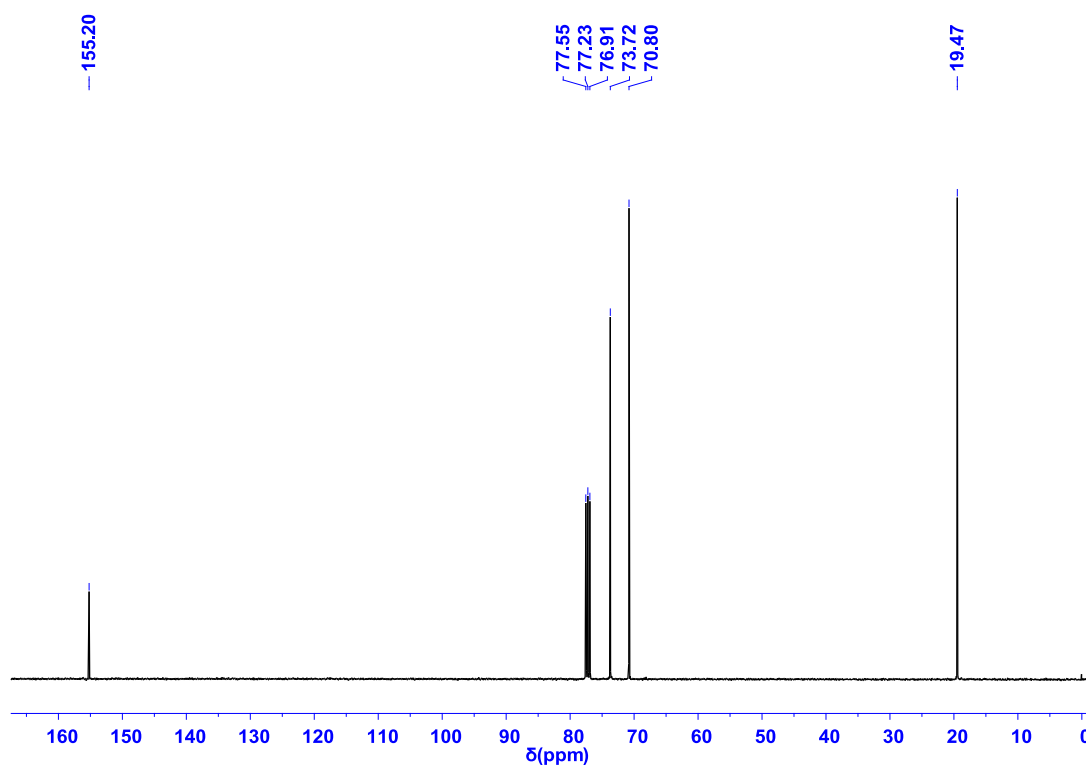


Figure S6. ^{13}C $\{^1\text{H}\}$ NMR of propylene carbonate in CDCl_3 .

PC: ^1H NMR (400 MHz, 25 °C, CDCl_3) δ 4.88–4.78 (m, 1H), 4.53 (dd, J = 8.4, 7.7 Hz, 1H), 3.99 (dd, J = 8.4, 7.2 Hz, 1H), 1.45 (d, J = 6.2 Hz, 3H). $^{13}\text{C}\{^1\text{H}\}$ NMR (101 MHz, 25 °C, CDCl_3) δ 155.2, 73.7, 70.8, 19.4.